Original articles

Characteristics of the formation and composition of $Al_xGa_{1-x}N$/AlN/por-Si/Si(111) heterostructures grown using a porous silicon buffer layer

A. S. Lenshin[1,2⊠], P. V. Seredin[1], D. S. Zolotukhin[1], A. N. Beltyukov[3], A. M. Mizerov[4], I. A. Kasatkin[5], A. O. Radam[1], E. P. Domashevskaya[1]

*[1]Voronezh State University,
1 Universitetskaya pl., Voronezh 394018, Russian Federation*

*[2]Voronezh State University of Engineering Technologies,
19 pr. Revolyutsii, Voronezh 394036, Russian Federation*

*[3]Udmurt Federal Research Centre of the Ural Branch of the Russian Academy of Sciences,
34 T. Baramzina ul., Izhevsk 426067, Russian Federation*

*[4]Alferov Federal State Budgetary Institution of Higher Education and Science Saint Petersburg National Research Academic University of the Russian Academy of Sciences,
Building 3, letter A, 8 Khlopin ul., Saint Petersburg 194021, Russian Federation*

*[5]Saint Petersburg State University,
7/9 Universitetskaya naberezhnaya, Saint Petersburg 199034, Russian Federation*

Abstract

In this work, we studied the efficiency of introducing nanoporous silicon as a buffer layer in the growth of $Al_xGa_{1-x}N$/AlN/Si(111) on a single-crystal silicon by molecular beam growth technology. We also considered its influence on the morphological characteristics and atomic composition of the surface layers of heterostructures. As determined by X-ray diffraction, microscopic, and X-ray photoelectron methods, the heterostructure grown on Si(111) *n*-type monocrystalline silicon wafer with nanoporous por-Si buffer layer has a more homogeneous epitaxial layer, and the surface morphology of the layer is also more homogeneous.

Keywords: Porous silicon buffer layer, Heterostructures, Epitaxy

---

⊠ Alexander S. Lenshin, e-mail: lenshinas@mail.ru

Condensed Matter and Interphases / Конденсированные среды и межфазные границы   2022;24(1): 51–58

A. S. Lenshin et al.   Characteristics of the formation and composition of Al$_x$Ga$_{1-x}$N/AlN/por-Si/Si(111)...

1. Introduction

The integration of III-N technology with existing silicon technology is highly promising for creating new types of microwave and optoelectronic devices. The use of silicon substrates for the growth of III-N heterostructures is advantageous due to their commercial availability and the high level of Si technology. The main problem of integrating the two technologies is the considerable mismatch of crystal lattice parameters and thermal expansion coefficients. This results in a large number of defects, uncontrolled fluctuations of solid solution composition, as well as peeling and cracking of heterostructures. An equally important problem in the production of high-power microwave nitride transistors is the heat removal from devices, which have a power dissipation of dozens of watts [1–5].

The latest way to solve these problems is to introduce various transition buffer layers into the III-N/Si(111) heterostructure. These are multi-period superlattices, layers of alternating 2D–3D morphology, or layers with gradually changing composition [6–7]. The thickness of the buffer layers can reach several tens of micrometres. The main methods for growing heterostructures for various devices are metalorganic vapour-phase epitaxy (MOVPE) and molecular beam epitaxy (MBE).

The aim of this study was to determine how introducing por-Si nanoporous silicon as a buffer layer in the growth of AlxGa1-xN/AlN/por-Si/Si(111) heterostructure influenced the structural-morphological characteristics and atomic composition of the surface layers. For this purpose, we used X-ray diffraction, microscopic, and X-ray photoelectron methods.
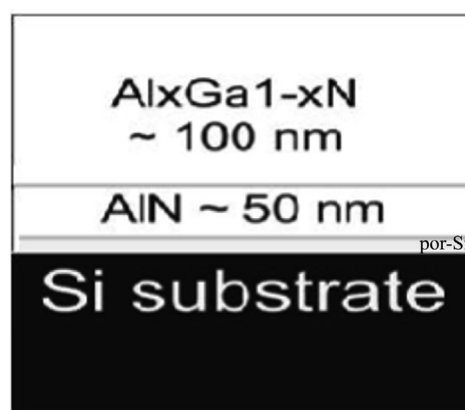
2. Experimental. Obtaining heterostructures by molecular beam epitaxy, structural and morphological research methods

We obtained Al$_x$Ga$_{1-x}$N/AlN/Si(111) heterostructures of two types, with a buffer por-Si layer and without it. They were grown simultaneously on a monocrystalline silicon Si(111) wafer by nitrogen-plasma-assisted molecular beam epitaxy (PA MBE) on a Veeco Gen 200 unit [7]. We used standard Si(111) wafers of monocrystalline silicon of KDB grade (boron-doped p-type silicon) as substrates for the growth of Al$_x$Ga$_{1-x}$N/AlN heterostructure layers. First, we formed nanoporous layers with a thickness of about 20 nm and an average pore diameter of less than 3 nm on half of the wafer surface using the original technique described in [8]. Immediately before growing the heterostructure, the wafers were annealed and nitrided for 30 min [9] in the growth chamber of the unit.

The formation of all the layers composing the heterostructures took place under metal enriched conditions. The growth rate was controlled and limited by the nitrogen flow, it was F_N~0.05 µm/h. An AlN buffer layer was formed on the substrate surface to prevent etching of the silicon substrate with liquid Ga and the formation of Ga-Si eutectic. After that, the growth of the main Al$_x$Ga$_{1-x}$N layer took place. Figure 1 shows the expected design set by the technological growth regime and the expected thickness of the layers of an Al$_x$Ga$_{1-x}$N/AlN/Si heterostructure with a buffer layer of nanoporous silicon.

The morphology of the grown heterostructures was examined with a JEOL JSM 6380 LV scanning electron microscope (SEM) and a SOLVER P47 PRO atomic force microscope (AFM). Statistical analysis of the surface morphology was performed using the NOVA software.

Fig. 1. The design of Al$_x$Ga$_{1-x}$N/AlN/Si heterostructure with nanoporous silicon buffer layer

Condensed Matter and Interphases / Конденсированные среды и межфазные границы   2022;24(1): 51–58

A. S. Lenshin et al.   Characteristics of the formation and composition of Al$_x$Ga$_{1-x}$N/AlN/por-Si/Si(111)...

The samples were studied by X-ray photoelectron spectroscopy (XPS) on a SPECS spectrometer. The depth of the XPS analysis of the sample surface is 1–2 nm.

When processing the measurement results, Shirley algorithms were used to determine the background line and subtract the background values. To determine the binding energy of the heterostructure elements, we used the C1s line of natural hydrocarbon impurities of the sample surface not subjected to special cleaning as a reference line, the binding energy Eb[C1s] = 285 eV. The core levels of the elements and their chemical state were determined using the X-ray photoelectron spectra database of the US National Institute of Standards [10].

The HR XRD data were obtained at 305 K on a Bruker D8 Discover diffractometer with a Ge220 monochromator.

3. Results and discussion

3.1. X-ray diffraction data

Figure 2 shows the results of X-ray diffraction in the ω–2θ geometry using the characteristic radiation of copper. It can be seen from the experimental data that the (111) diffraction line of the Si(111) silicon substrate is the most intense on the scans of both heterostructures. In addition, both scans show high-intensity reflexes (0002) from the basic plane of the hexagonal unit cell, which belong to the Al$_x$Ga$_{1-x}$N solid solution with a hexagonal structure. The fact that the diffractogram of the heterostructure with por-Si sublayer (dotted curves in Fig. 2) shows only the reflection from the basic plane (0002) suggests the monocrystalline state of the epitaxial film.

The diffractogram of the heterostructure grown on the c-Si(111) substrate without a porous sublayer (solid curves in Fig. 2) shows the reflection from the plane (11–20) of the Al$_x$Ga$_{1-x}$N solid solution. This reflection may be due to growth of Al$_x$Ga$_{1-x}$N solid solution columns in the <11–20> direction. Similar reflections were not observed in the ω-2θ scan of the heterostructure with a porous sublayer, indicating greater homogeneity and perfection of its crystalline structure.

3.2. Sample morphology studied by scanning electron and atomic force microscopy.

Fig. 3. shows SEM images of the surface of heterostructures obtained on monocrystalline silicon substrates (a) and using a buffer sublayer of porous silicon (b).

The surface of the samples exhibits sub-micron inhomogeneities caused by the columnar
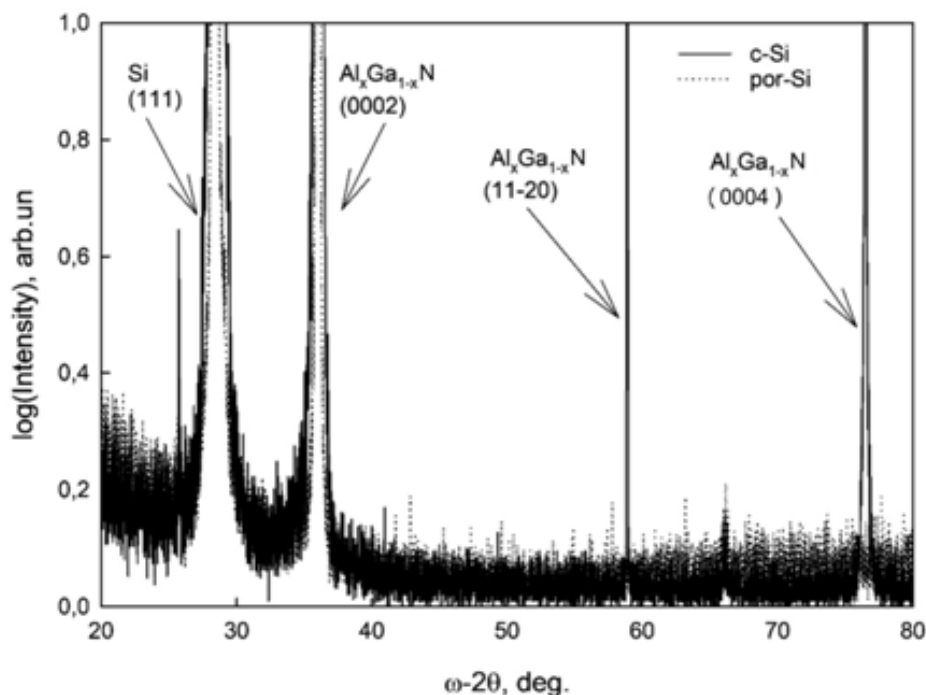
Fig. 2. XRD patterns of Al$_x$Ga$_{1-x}$N/AlN heterostructures grown on c-Si(111) (dotted line) and por-Si/c-Si(111) (solid line) wafers

Condensed Matter and Interphases / Конденсированные среды и межфазные границы   2022;24(1): 51–58

A. S. Lenshin et al.   Characteristics of the formation and composition of Al$_x$Ga$_{1-x}$N/AlN/por-Si/Si(111)...
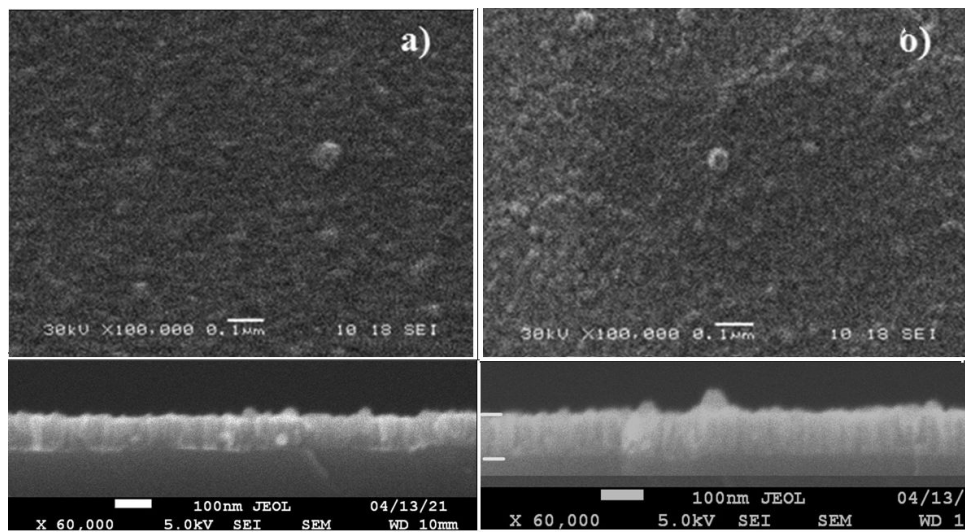
Fig. 3. SEM images of the surface and chipping of heterostructures: a) on the Al$_x$Ga$_{1-x}$N/AlN/Si(111) monocrystalline silicon wafer; b) on the Al$_x$Ga$_{1-x}$N/AlN/por-Si/Si(111) wafer with por-Si buffer layer

film structure observed in SEM images of the chipped samples. We had observed a similar columnar film structure in In$_x$Ga$_{1-x}$N/Si(111) heterostructures [11–12]. We compared the morphology of the two types of heterostructures, with and without the por-Si sublayer, and saw that the heterostructure grown on a porous layer had a smaller spread in the sizes of the surface inhomogeneities. So, its film structure was more homogeneous compared to the heterostructure grown without the buffer layer. This conclusion confirmed the above XRD data.

The analysis of the profile SEM images showed that the actual thickness of the heterostructure layers coincided with those specified in the technological procedure. The lateral size distribution of surface inhomogeneities caused by the columnar structure of the film was determined by analysing AFM images (Figure 4).

Fig. 4 shows the AFM surface images and size distribution profiles of two Al$_x$Ga$_{1-x}$N/AlN/Si(111) heterostructures grown directly on a c-Si(111) wafer and with a pre-formed buffer layer of porous silicon. The samples with the por-Si buffer layer have a smaller spread in the size of inhomogeneities compared to the heterostructure grown on crystalline silicon (Fig. 4a). The average inhomogeneity size on the surface of the samples grown with the por-Si buffer layer is ~100 nm. Al$_x$Ga$_{1-x}$N/AlN/Si samples grown on crystalline silicon show two maxima of nanocolumn size distribution of ~65 and 130 nm (Fig. 4c).
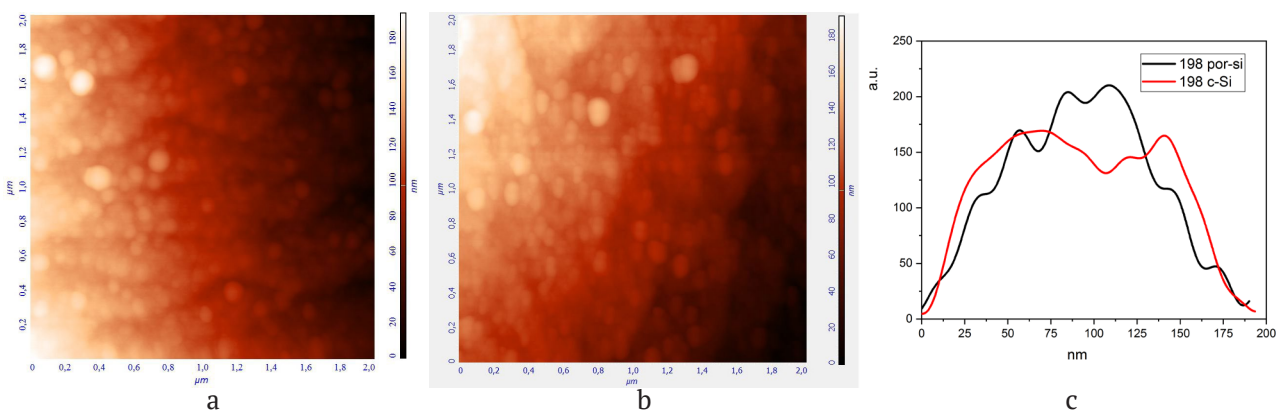
Fig. 4. AFM surface images of Al$_x$Ga$_{1-x}$N/AlN/Si heterostructures grown: on the monocrystalline c-Si(111) wafer (a), on the por-Si/s-Si(111) wafer with a porous sublayer (b), and size distribution profiles of inhomogeneities on their surface (c)

Condensed Matter and Interphases / Конденсированные среды и межфазные границы   2022;24(1): 51–58

A. S. Lenshin et al.   Characteristics of the formation and composition of Al$_x$Ga$_{1-x}$N/AlN/por-Si/Si(111)...

3.3. Atomic composition of the surface of heterostructures as determined by X-ray photoelectron spectroscopy (XPS).

Figures 5 and 6 show XPS images of Al 2p, Ga 2p, and N1s core levels for heterostructures grown directly on monocrystalline silicon c-Si(111) (Fig. 5) and with a porous sublayer (Fig. 6). Table 1 shows the values of the binding energy determined with an accuracy of 0.05 eV and the half width values based on XPS study of the core levels for the two heterostructures.

XPS spectra analysis showed that on the surface of both heterostructures Al and Ga atoms formed chemical bonds with nitrogen. The binding energy (and half-width) of the core level spectra of all three elements in the Al$_x$Ga$_{1-x}$N solid solution were practically identical. The values were close to the binding energy of aluminium

and gallium in nitrides [10]. In addition, the Al 2p spectra demonstrated the contribution of the low-intensity component of oxidised aluminium Al$_2$O$_3$ (*E*b = 75.5 eV), formed on the surface of the samples when exposed to air. The Ga 2p**3**/2 spectrum showed no similar component, but that may be due to the nitrogen N KLL Auger line superimposed on the low-energy part of the gallium spectrum. The binding energy values of the N1s nitrogen spectra correspond to Al and Ga nitrides [10]. In addition, a low-energy hydride component was observed in the nitrogen spectra, apparently it was due to the residual reagents on the surface of heterostructures (NH$_3$ type bonds, *E*b = 398.7 eV [10]).

By analogy with studies [13,14], the aluminium content of the film can be calculated using relation (1):
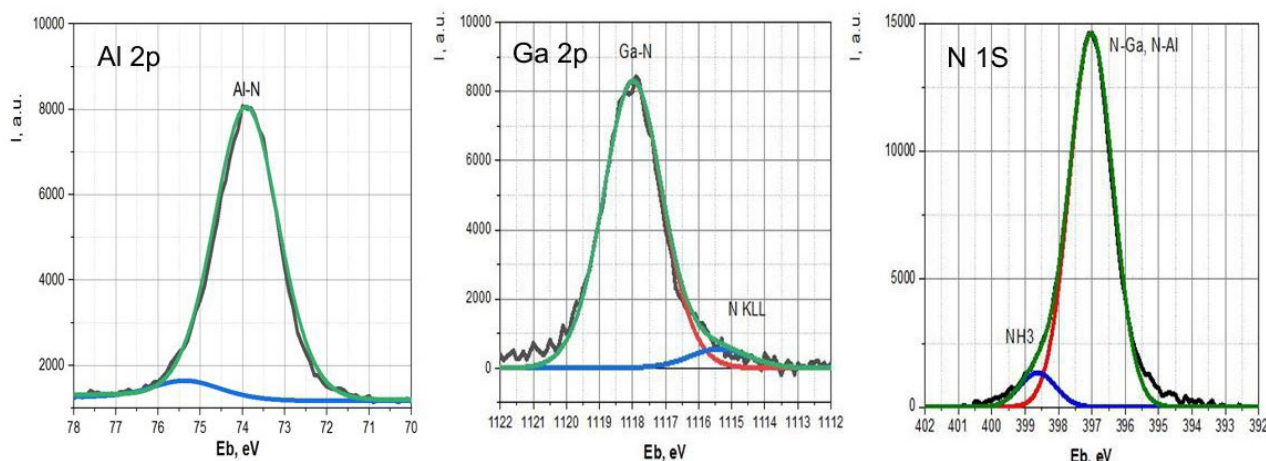
Fig. 5. XPS of Al 2p, Ga 2p**3**/2**,** and N1s in Al$_x$Ga$_{1-x}$N/AlN/Si(111) heterostructures, grown on the monocrystalline silicon Si(111) wafer
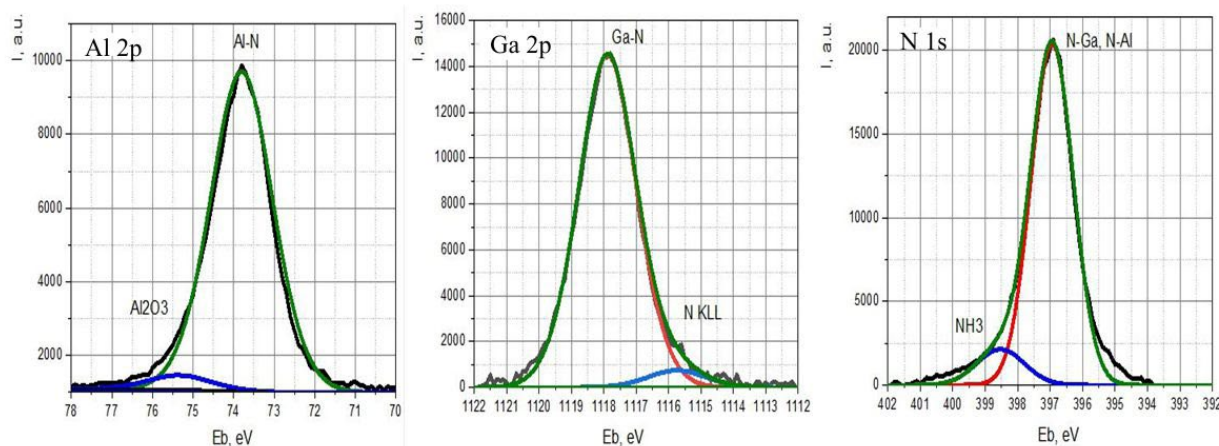
Fig. 6. XPS of Al 2p, Ga 2p**3**/2**,** and N1s in Al$_x$Ga$_{1-x}$N/AlN/por-Si/Si(111) heterostructures grown on monocrystalline silicon wafer with a buffer layer of porous silicon

Condensed Matter and Interphases / Конденсированные среды и межфазные границы 2022;24(1): 51–58

A. S. Lenshin et al. Characteristics of the formation and composition of Al$_x$Ga$_{1-x}$N/AlN/por-Si/Si(111)...

Table 1. Binding energy and half-width values by XPS of Al 2p, Ga 2p3/2, and N 1S core levels for heterostructures grown on c-Si(111) and on por-Si/c-Si(111)

	Binding energy, eV/ Half-width, eV					
	Al2p		Ga2p3/2		N1s	
Al$_x$Ga$_{1-x}$N/AlN /c-Si	73.80	1.64	1117.92	2.10	396.97	1.55
Al$_x$Ga$_{1-x}$N/AlN /por-Si/c-Si	73.91	1.72	1117.87	2.15	396.93	1.56
AlN [10]	73.90					
GaN [10]			1117.80			
GaN [10]					397.0	
AlN [10]					397.30	

$$x_{Al} = \frac{I_{Al_2p_3} / F_{Al_2p_3}}{(I_{Al_2p_3} / F_{Al_2p_3} + I_{Ga_2p_3} / F_{Ga_2p_3})}, \qquad (1)$$

where I is the integral intensity of the photoelectron maxima of the corresponding lines in the spectrum and F is the sensitivity factor ($F_{Ga2}p_3 = 2.75$ and $F_{Al2}p_3 = 0.54$). Based on relation (1), we determined the Al atom concentration values in solid solution. They were $x_{a\_cryst} = 0.49$ for samples of Al$_x$Ga$_{1-x}$N/AlN/Si(111) grown directly on monocrystalline silicon and $x_{a\_por} = 0.54$ for samples of Al$_x$Ga$_{1-x}$N/AlN/Si/por-Si/Si(111) grown using a porous buffer layer. It coincided quite well with the expected technological values of x-0.50 specified during synthesis. The slight difference in the values of x of the two heterostructures may be due to their minor structural and morphological differences.

4. Conclusions

For the first time, Al$_x$Ga$_{1-x}$N/AlN/por-Si/Si (111) heterostructures were formed by nitrogen-plasma-assisted molecular beam epitaxy using a buffer layer of por-Si porous silicon.

X-ray diffraction and electron microscopy methods showed that the formation of Al$_{0.54}$Ga$_{0.46}$N solid solution on a buffer layer of porous silicon results in a more homogeneous size distribution and orientation in the basic direction of the solid solution nanocolumns compared to the similar solid solution Al$_{0.49}$Ga$_{0.51}$N, grown simultaneously on the same plate of monocrystalline silicon without porous layer under the same technological conditions.

The slight shift of ~ 5 % towards Al demonstrated by the surface composition of the solid solution on the substrate with a buffered porous layer may be due to the more homogeneous structural and morphological characteristics of this heterostructure.

Author contributions

Lenshin A. S. – scientific guidance, research concept, sample synthesis, text writing, and final conclusions. Zolotukhin D. S. – text writing, final conclusions. Beltyukov A. N. – measurements, text writing. Seredin P. V. – measurements, text writing. Mizerov A. M. – sample synthesis, text writing. Kasatkin I. A. – measurements, text writing. Radam A. O. – measurements. Domashevskaya E. P. – text editing, final conclusions.

Conflict of interests

The authors declare that they have no known competing financial interests or personal relationships that could have influenced the work reported in this paper.

References

1. Ho V. X., Al Tahtamouni T. M., Jiang H. X., Lin J. Y., Zavada J. M., Vinh N.Q. Room-temperature lasing action in GaN quantum wells in the infrared 1.5 µm region. *ACS Photonics*. 2018;5: 1303–1309. https://doi.org/10.1021/acsphotonics.7b01253

2. Laurent T., Manceau J.-M., Monroy E., Lim C. B., Rennesson S., Semond F., Julien F. H., Colombelli R. Short-wave infrared (λ = 3 µm) intersubband polaritons in the GaN/AlN system. *Applied Physics Letters*. 2017;110: 131102. https://doi.org/10.1063/1.4979084

3. Ajay A., Lim C. B., Browne D. A., Polaczynski J., Bellet-Amalric E., den Hertog M. I., Monroy E. Intersubband absorption in Si- and Ge-doped GaN/AlN heterostructures in self-assembled nanowire and 2D layers. *Physica Status Solidi B*. 2017;254: 1600734. https://doi.org/10.1002/pssb.201600734

4. Gkanatsiou A. A., Lioutas Ch. B., Frangis N., Polychroniadis E. K., Prystawko P., Leszczynski M. Electron microscopy characterization of AlGaN/GaN

Condensed Matter and Interphases / Конденсированные среды и межфазные границы 2022;24(1): 51–58

A. S. Lenshin et al. Characteristics of the formation and composition of Al$_x$Ga$_{1-x}$N/AlN/por-Si/Si(111)...

heterostructures grown on Si (111) substrates. *Superlattices and Microstructures*. 2017;103: 376–385. https://doi.org/10.1016/j.spmi.2016.10.024

5. Oh J-T., Moon Y-T., Jang J-H., Eum J-H., Sung Y-J., Lee S. Y., Song J-O., Seong T-Y. High-performance GaN-based light emitting diodes grown on 8-inch Si substrate by using a combined low-temperature and high-temperature-grown AlN buffer layer. *Journal of Alloys and Compounds*. 2018;732: 630–636. https://doi.org/10.1016/j.jallcom.2017.10.200

6. Sugawara Y., Ishikawa Y., Watanabe A., Miyoshi M., Egawa T. Observation of reaction between a-type dislocations in GaN layer grown on 4-in. Si(111) substrate with AlGaN/AlN strained layer superlattice after dislocation propagation. *Journal of Crystal Growth*. 2017;468: 536–540. https://doi.org/10.1016/j.jcrysgro.2016.11.010

7. Mizerov A. M., Timoshnev S. N., Sobolev M. S., Nikitina E. V., Shubina K. Yu., Berezovskaia T. N., Shtrom I. V., Bouravleuv A. D. Features of the initial stage of GaN growth on Si(111) substrates by nitrogen-plasma-assisted molecular-beam epitaxy. *Semiconductors*. 2018;52(12), 1529-1533. https://doi.org/10.1134/S1063782618120175

8. Kukushkin S. A., Mizerov A. M., Osipov A. V., Redkov A. V., Timoshnev S. S. Plasma assisted molecular beam epitaxy of thin GaN films on Si(111) and SiC/Si(111) substrates: Effect of SiC and polarity issues. *Thin Solid Films*. 2018;646: 158–162. https://doi.org/10.1016/j.tsf.2017.11.037

9. Lenshin A. S., Kashkarov V. M., Domashev-skaya E. P., Bel'tyukov A. N., Gil'mutdinov F. Z. Investigations of the composition of macro-, micro- and nanoporous silicon surface by ultrasoft X-ray spectroscopy and X-ray photoelectron spectroscopy. *Applied Surface Science*. 2015;359: 550–559. https://doi.org/10.1016/j.apsusc.2015.10.140

10. *NIST X-ray Photoelectron Spectroscopy Database*. Available at: https://srdata.nist.gov/xps/

11. Seredin P. V., Goloshchapov D. L., Lenshin A. S., Mizerov A. M., Zolotukhin D. S. Influence of por-Si sublayer on the features of heteroepitaxial growth and physical properties of InxGa1-xN/Si(111) heterostructures with nanocolumn morphology of thin film. *Physica E: Low-dimensional Systems and Nanostructures*. 2018;104: 101–110. https://doi.org/10.1016/j.physe.2018.07.024

12. Seredin P. V., Lenshin A. S., Mizerov A. M., Leiste H., Rinke M. Structural, optical and morphological properties of hybrid heterostructures on the basis of GaN grown on compliant substrate por-Si(111). *Applied Surface Science*. 2019;476: 1049–1060. https://doi.org/10.1016/j.apsusc.2019.01.239

13. Fang Z. L., Li, Q. F. Shen X. Y., Cai J. F., Kang J. Y., Shen W. Z., Modified InGaN/GaN quantum wells with dual-wavelength green-yellow emission. *Journal of Applied Physics*. 2014;115(4): 043514. https://doi.org/10.1063/1.4863208

14. Seredin P. V., Lenshin A. S., Zolotukhin D. S., Goloshchapov D. L., Mizerov A. M., Arsentyev I. N., Beltyukov A. N. Investigation into the influence of a buffer layer of nanoporous silicon on the atomic and electronic structure and optical properties of A^{III}N/por-Si heterostructures grown by plasma-activated molecular-beam epitaxy. *Semiconductors*. 2019;53 (7): 993–999. https://doi.org/10.1134/S1063782619070224

Information about the authors

Alexander S. Lenshin, DSc in Physics and Mathematics, leading researcher at the Department of Solid State Physics and Nanostructures, Voronezh State University; Associate Professor, Voronezh State University of Engineering Technologies (Voronezh, Russian Federation).

https://orcid.org/0000-0002-1939-253X
lenshinas@phys.vsu.ru

Pavel V. Seredin, DSc in Physics and Mathematics, Head of the Department of Solid State Physics and Nanostructures, Voronezh State University (Voronezh, Russian Federation).

https://orcid.org/0000-0002-6724-0063
paul@phys.ru

Dmitry S. Zolotukhin, PhD student at the Department of Solid State Physics and Nanostructures, Voronezh State University (Voronezh, Russian Federation).

https://orcid.org/0000-0002-9645-9363
zolotuhin@phys.vsu.ru

Artemy N. Beltyukov, PhD in Physics and Mathematics, Senior Researcher at the Udmurt Federal Research Center of the Ural Branch of the Russian Academy of Sciences (Izhevsk, Russian Federation).

https://orcid.org/0000-0002-7739-7400
beltukov.a.n@gmail.com

Andrey M. Mizerov, PhD in Physics and Mathematics, Leading Researcher at the Laboratory of Nanoelectronics, Alferov Federal State Budgetary Institution of Higher Education and Science Saint Petersburg National Research Academic University of the Russian Academy of Sciences (Saint Petersburg, Russian Federation).

https://orcid.org/0000-0002-9125-6452
andreymizerov@rambler.ru

Igor A. Kasatkin, PhD in Geology and Mineralogy, leading specialist in high resolution X-ray diffractometry, Saint Petersburg State University, Research Centre for X-ray Diffraction Studies (Saint Petersburg, Russian Federation).

https://orcid.org/0000-0001-9586-5397
igor.kasatkin@spbu.ru

Condensed Matter and Interphases / Конденсированные среды и межфазные границы   2022;24(1): 51–58

A. S. Lenshin et al.   Characteristics of the formation and composition of Al$_x$Ga$_{1-x}$N/AlN/por-Si/Si(111)…

Ali O. Radam, PhD student at the Department of Solid State Physics and Nanostructures, Voronezh State University (Voronezh, Russian Federation).
https://orcid.org/0000-0002-1072-0816
radam@phys.vsu.ru

Evelina P. Domashevskaya, DSc in Physics and Mathematics, Professor at the Department of Solid State Physics and Nanostructures, Voronezh State University (Voronezh, Russian Federation).
https://orcid.org/0000-0002-6354-4799
ftt@phys.ru